Dynamic Behavior Issues in Three-Way Catalyst Modeling

Grigorios C. Koltsakis and Anastasios M. Stamatelos
Laboratory of Applied Thermodynamics, Aristotle University of Thessaloniki, 540 06 Thessaloniki, Greece

Mathematical modeling of three-way catalytic converter (3WCC) operation is used increasingly in automotive catalyst and converter systems optimization. The majority of these models employ a ''quasi-steady'' approach in the reaction kinetics computations, which is useful in predicting real-world performance of the catalyst. However, certain improvements produced by the application of specially tuned redox oscillations cannot be predicted. The approach presented embodies certain types of dynamic phenomena in an existing 3-WCC quasi-steady model. The dynamic model based on this approach is validated against data in the literature and experimental results. It is confirmed that the catalyst behavior under dynamic exhaust composition conditions significantly differs from predictions under the quasi-steady-state assumption. Oxygen storage and the transient character of water gas shift reaction affect dynamic behavior. The results of this investigation encourage further application of mathematical modeling in such areas as lambda control strategy optimization that lie beyond the scope of traditional 3WCC models.

Introduction

The three-way catalytic converter (3WCC), an indispensable device for the control of CO, HC, and NO_x emissions of gasoline engines, is a chemical reactor operating at highly transient conditions. The temperature, flow rate, and composition of the exhaust gas flowing through the converter honeycomb monolith change significantly according to the driving mode, with a typical time scale of several seconds. At the same time, the closed-loop control of the fuel-management system induces further, more severe, transients of the feed gas composition with a typical time scale of less than a second. The latter effect is attributed to the interaction between the engine and the lambda sensor (Bozek et al., 1992), which is used as a feedback control signal for the fuel injection system in order to ensure that a stoichiometric fuel-air mixture is supplied in the engine cylinders. However, the system's response lag (mainly attributable to the exhaust-gas travel time and the sensor's response delay) causes the air-to-fuel (A/F) ratio to oscillate around the stoichiometric value with the limit-cycle frequency of the control system.

Correspondence concerning this article should be addressed to A. M. Stamatelos.

The behavior of the 3WCC under such dynamic conditions therefore presents a great deal of practical interest. Since the beginning of the previous decade, it has been recognized that the 3-way catalyst efficiency is significantly affected when the composition of the feed gas is oscillating with different amplitudes and frequencies (Shulman et al., 1982; Herz et al., 1983; Taylor and Sinkevitch, 1983; Schlatter et al., 1983; Barshad and Gulari, 1985; Matsunaga et al., 1987). This behavior is mainly attributed to the ability of some washcoat components to be periodically oxidized and reduced, depending on the exhaust-gas redox environment. For example, the activity of the noble metals Pt, Pd, and Rh depends on their oxidation state, and is lowered for higher oxidation levels (Diwell et al., 1991; Nunan et al., 1991).

The advent of stricter U.S. and European emission standards has increased the need for reliable 3WCC models that support the design of demanding exhaust systems. A number of mathematical models working in this direction are already presented in the literature and employed in optimization procedures (Oh and Cavendish, 1985; Pattas et al., 1994; Siemund et al., 1996). On the other hand, the research on the effect of oscillating A/F has been restricted mainly to experimental testing and empirical explanations of results. In a number of

previous articles, a mathematical modeling approach was presented, aiming at the simulation of the transient adsorption, desorption, and surface reactions occurring in a 3-way catalyst under oscillating A/F conditions with simple gas mixtures (Herz and Marin, 1980; Racine and Herz, 1992; Hoebink et al., 1997). Such models are considered difficult to apply in realistic automotive conditions, where many interacting exhaust species are present and participating in many heterogeneous reactions.

In this work, an alternative approach to model highly transient phenomena in catalytic converters is presented. First, the most important dynamic phenomena are recognized based on research in the literature. Simple, tunable models are developed to describe these phenomena, which are then embodied in a ''quasi-steady'' model. A series of simple published experimental tests are employed to support the validity of the approach and tune the basic kinetic parameters involved.

Having established the mathematical model, the transient behavior of the 3WCC is studied during A/F scanning from lean-to-rich exhaust environment and vice versa. The effect of A/F oscillations superimposed on the A/F scan is also studied using experimental measurements and model computations. The model predictions are also compared to those computed with the ''quasi-steady'' assumption. The ability of the model to predict catalyst behavior under oscillating A/F conditions is discussed.

Transient 3 WCC Model

As mentioned in the Introduction, a previously developed 3WCC mathematical model will be extended and equipped with submodels of the main dynamic phenomena. A detailed description of the basic model can be found in Koltsakis et al. (1997). The basic features of the ''quasi-steady'' mathematical model can be summarized as follows:

- Computation of the convective heat and mass transfer from the exhaust gas to the catalytic surface. A ''film approach'' is adopted employing mean bulk values for the gas-phase and solid–gas interface values for the solid-phase species concentrations.
- Computation of the heterogeneous chemical reactions taking place on the catalytic surface based on Langmuir–Hinshelwood-based rate expressions. ''Lumping'' of surface adsorption/desorption and pore diffusion phenomena in the kinetic-rate expressions.
- The two-dimensional (2-D) transient temperature field in the cylindrical converter is computed taking the heat conduction in the substrate and the surrounding insulation, and the heat losses to the surroundings via convection and radiation into account.

Detailed formulation of the energy and mass balance equations, as well as the solution procedure followed, are described in detail by Koltsakis et al. (1997). As with all quasi-steady models the computation of the species concentrations and the reaction rates is based on the equation of the diffusion and reaction rates for each species j:

$$\dot{n}_{i,j}(c_{g,i,j}, c_{s,i,j}) = R_{i,j}(\bar{c}_{s,i}, T_{s,i}). \qquad (1)$$

The lefthand side of the equation concerns the mass diffusion rate resulting from the concentration gradient between the gas bulk phase and wall. The reaction rates R_j (righthand side) are nonlinear functions of the local temperature and composition at the gas–solid interface. The reactions, kinetic expressions, and kinetic constants used in the present model are listed in Appendix A (Koltsakis et al., 1998).

According to Eq. 1, the rates of reaction and mass transfer to the catalytic surface are always in equilibrium, implying that there is no species accumulation phenomena on the solid catalytic surface. This assumption is realistic for steady-state operation, but not necessarily so for an operation under highly transient temperature and composition conditions. In the latter case, employment of Eq. 1 with Langmuir–Hinshelwood-type expressions for the reaction rates, would probably not be sufficient. In order to account for the effects of transient adsorption–desorption and heterogeneous reaction phenomena, the kinetic model should include the detailed computation of the time-dependent surface coverage of each species on the active sites. Such models have been presented by a number of researchers (Oh et al., 1986; Nievergeld et al., 1994) for the case of a 1-D isothermal reactor with simple gas mixtures (up to three reacting species). These models aimed at studying the effects of the oscillatory equivalence ratio on catalyst performance. However, the number of kinetic parameters needed for such a task are numerous and very difficult to estimate.

In our model, the quasi-steady approach expressed by Eq. 1 is retained, while highly transient effects, which are probably the most dominant for practical application cases, are taken into account. Specifically, the phenomena considered to be of major importance are (Herz and Sell, 1985; Su and Rothchild, 1986; Koltsakis, 1996):

- The oxygen storage and release phenomena in the washcoat are described by the dynamic redox activity of the cerium oxides present in the catalytic layer. Tunable kinetic rate expressions are employed to represent catalyst performance in a wide range of temperature and redox environments.
- Rh activity dependence on Rh oxidation state, as regards the water–gas reaction, is considered with a dynamic oxidation–reduction model.

This aims at keeping model complexity, and thus flexibility, to acceptable levels, while at the same time profiting from the available experience regarding Langmuir–Hinshelwood kinetic rate expressions for three-way catalysts.

Oxygen Storage Submodel

The washcoat component, that seems to play the most important role in such dynamic oxidation–reduction phenomena is ceria. Ceria is normally present in large quantities in the washcoat [order of 30% weight or 1,000 g/ft^3 (35 kg/m^3)] and has multiple functions: stabilization of the washcoat layer and improvement of thermal resistance, enhancement of precious-metal catalytic activity, and functions as an oxygen storage component.

The function of cerium as an oxygen storage component is based on its ability to form both three and four-valent oxides (Herz, 1981). Under net oxidizing conditions, the following Ce oxide reaction is the most representative for the realiza-

tion of oxygen storage:

$$Ce_2O_3 + 1/2\,O_2 \rightarrow 2CeO_2. \tag{2}$$

This reaction represents the storage of an oxygen atom by increasing the oxidation state of Ce_2O_3.

On the other hand, the CeO_2 may function as an oxidizing agent of the exhaust-gas species under net reducing conditions according to the following reactions:

$$CO + 2CeO_2 \rightarrow Ce_2O_3 + CO_2 \tag{3}$$

$$C_xH_y + 2\left(x + \frac{y}{2}\right)CeO_2 \rightarrow \left(x + \frac{y}{2}\right)Ce_2O_3 + xCO + \frac{y}{2}H_2O. \tag{4}$$

Each of the preceding reactions denotes the release of an oxygen atom, which is made available to react with a reducing species of the exhaust gas (CO or HC). We define the auxiliary number ψ as

$$\psi = \frac{2 \times \text{mol } CeO_2}{2 \times \text{mol } CeO_2 + \text{mol } Ce_2O_3}, \tag{5}$$

which can be considered as the fractional extent of the oxidation of the oxygen storage component. The extent of oxidation is changing continuously during transient converter operation and is affected by the relative reaction rates of the reactions expressed in Eqs. 2–4.

The rate of the reaction in Eq. 2 (oxidation rate) is expected to be proportional to the available active sites of ''reduced-state'' cerium oxides, which is expressed by the factor $\Psi_{cap}(1-\psi)$. The rate also should be dependent on the prevailing oxygen concentration at the gas–solid interface. The linear dependence on O_2 concentration is considered as a realistic assumption. The oxidation reaction rate is thus

$$R_{ox} = k_{ox}(T)c_{s,O_2}\Psi_{cap}(1-\psi), \tag{6}$$

where k_{ox} is a characteristic rate constant, which exhibits an Arrhenius-type dependence on temperature:

$$k_{ox} = A_{ox} \cdot e^{-E_{ox}/RT}. \tag{7}$$

Analogous considerations are made for the reduction reactions rates. Here, the rates are expected to be directly proportional to $\Psi_{cap}\psi$, and should exhibit a dependence on the local carbon oxide (CO) and hydrocarbon (HC) concentration, respectively:

$$R_{red,CO} = k_{red,CO}(T)c_{CO}\Psi_{cap}\psi \tag{8}$$

$$R_{red,HC} = k_{red,HC}(T)c_{HC}\Psi_{cap}\psi \tag{9}$$

$$R_{red} = R_{red,CO} + R_{red,HC}, \tag{10}$$

with

$$k_{red,CO} = A_{red,CO} \cdot e^{-E_{red}/RT} \tag{11}$$

$$k_{red,HC} = A_{red,HC} \cdot e^{-E_{red}/RT}. \tag{12}$$

The variation of the oxidation extent ψ should be computed at each location by the following differential equation:

$$\frac{d\psi}{dt} = -\frac{1}{\Psi_{cap}}(R_{red} - R_{ox}), \tag{13}$$

which is solved numerically by the implicit Euler method for each node, along the catalyst channels.

Rh Redox Submodel

The water–gas shift reaction

$$CO + H_2O \rightarrow CO_2 + H_2$$

consumes further CO, leaving more oxygen available for hydrocarbon oxidation. According to findings from other research works, this reaction can be catalyzed by Rh or Pd, provided that the catalyst surface has undergone some extent of oxidation (Schlatter and Mitchell, 1980; Herz and Sell, 1985; Dictor, 1987; Barbier and Duprez, 1992).

The reversible oxidation–reduction process of the active catalyst is taken into account in the mathematical model by a submodel for the computation of active metal oxidation state. Assuming that the active metal for the water–gas reaction is Rh, we define θ_{Rh} as the fraction of the Rh sites that are oxidized (active). We consider that the Rh oxidation and reduction rates can be expressed by the following general relations:

$$R_{ox} = (1-\theta_{Rh}) \cdot k_{Rh,ox} \cdot f_{ox}(\bar{c}_j) \tag{14}$$

$$R_{red} = \theta_{Rh} \cdot k_{Rh,red} \cdot f_{red}(\bar{c}_j). \tag{15}$$

The parameters $k_{Rh,ox}k_{Rh,red}$ are exponential functions of temperature (an Arrhenius-type dependence on temperature is assumed). The functions $f_{ox}(\bar{c}_j)$, $f_{red}(\bar{c}_j)$ denote the dependence of the reaction rates on the availability of oxidizing–reducing species. We can accept that the reaction rates are proportional to the oxygen atom equivalents of each species. Therefore;

$$f_{ox}(\bar{c}_j) = 2c_{O_2} + c_{NO} \tag{16}$$

$$f_{red}(\bar{c}_j) = c_{CO} + c_{H_2} + \alpha_f c_{(HC)_f} + \alpha_s c_{(HC)_s}. \tag{17}$$

Having defined the oxidation and reaction rates, the temporal evolution of θ_{Rh} is given by the following first-order differential equation:

$$\frac{d\theta_{Rh}}{dt} = R_{ox} - R_{red},$$

which is solved by the implicit Euler method.

Step-Composition Changes

In this section, we examine the ability of the dynamic model to simulate transient phenomena dealing with oxygen storage and water–gas reaction during step feed gas composition changes. For this purpose, the published experimental findings of Herz and Sell (1985) are exploited. The experiments were conducted with a 2,620-cm^3 (1,370-g) catalyst installed in a 5.7-L engine. The GHSV was 50,000 h^{-1}, and the exhaust-gas temperature entering the converter between 740 and 750 K. The exhaust-gas composition as a function of the A/F ratio is given in Table 1. Stoichiometry corresponds to an A/F value of 14.75.

As is described below, two different sets of experiments are conducted, each with three different catalysts. The first catalyst contains Pt and Rh as the catalytically active noble metals and Ce as an oxygen storage component. The second catalyst, which contains only Pt/Ce is expected to show good oxygen storage properties and negligible potential for water–gas reaction catalysis. On the contrary, the third catalyst, which contains only Pt/Rh, is expected to be active for water–gas reaction, but without oxygen storage abilities. All catalysts contained 2.6 μmol/g Pt; Rh concentration in the Pt/Rh and the Pt/Rh/Ce catalysts was 0.5 μmol/g; and Ce concentration in the Pt/Ce and the Pt/Rh/Ce catalysts was 143 μmol/g.

In the first experiment, a step A/F change from 15.1 (lean) to 14.1 (rich) was imposed and the CO concentration at the catalyst exit was recorded as a function of time. The measured responses are presented in Figure 1a. The expected CO response, assuming quasi-steady catalyst behavior, is indicated by dotted lines. During the first 20 s after the step-composition change, an increased CO conversion compared with the steady-state case was observed for all three catalysts. Differences in the CO response between the three catalysts are clear. The number in parentheses on each plot in Figure 1a is the maximum amount of CO (μmol/g catalyst) that could be removed by storage/release processes on the noble metals and ceria. The number above the parentheses denotes the actually removed amount of CO. The discrepancy between these two numbers demonstrates an enhanced CO removal, which is attributed to the water–gas shift reaction.

According to the previous discussion, the Pt/Rh catalyst is simulated with no oxygen storage capabilities. Based on the results of the step A/F change experiment (Figure 1a), the kinetics of the Rh redox reactions are tuned by trial and error in order to get an acceptable match between experiment and simulation. Similarly, the measurement of the Pt/Ce catalyst (no activity regarding the water–gas reaction) is employed to tune the oxygen storage submodel kinetics. The values estimated from the tuning process are given in the table in Appendix A. It can be seen from the preexponential factors in the table that for both phenomena the oxidation rates are higher than the respective reduction rates. This is in agreement with earlier findings in the literature (Herz, 1987).

Table 1. Exhaust Gas Composition for the Experiments and Simulations for the Dynamic Behavior Study under Step Composition Changes

Vol. %	A/F = 14.1	A/F = 15.1
CO	1.3	0.28
HC	0.062	0.04
NO	0.099	0.1
O_2	0.28	1.1
H_2	0.43	0.093

Source: Herz and Sell (1985).

The Pt/Rh/Ce catalyst is modeled using the estimated kinetic constants for both phenomena. The results of the computational simulation for all three catalysts are presented in Figure 1b. The model ability to simulate the transient behavior of CO conversion in these cases is quite satisfactory.

In order to interpret the results, the stored oxygen and the Rh oxidation extent (averaged over the converter) are presented as functions of time for the three test cases in Figure 1c. It can be initially observed that the time constants involved with these phenomena are of the same order of magnitude.

In the second experiment, the engine runs at a constant operation point with A/F = 14.1. A lean excursion (A/F = 15.1) is imposed for 1 s, and the engine returns to the previous rich operating point. The experimental results are presented in Figure 2a. The high oxygen availability after the onset of lean explains the resulting sudden drop in CO concentration. Hence, a quasi-steady catalyst behavior would show a sudden increase in CO concentration after switching again to rich (dashed lines).

The catalyst response is simulated based on the kinetics acquired from the previous experimental test case, and the results are presented in Figure 2b. For the Pt/Ce catalyst the CO response at catalyst exit presents only minor differences compared to the expected quasi-steady behavior. This indicates that the relatively short duration of the lean excursion was not enough for the catalyst to store sufficient oxygen, which would contribute after switching to the rich operating mode. The relevant calculation shows that only 20% of the oxygen storage capacity is activated during the test (Figure 2c).

On the other hand, the Pt/Rh catalyst shows significant activity after the A/F switch to its initial rich value. This implies that the 1-s duration of the lean excursion was enough to bring Rh to a substantial oxidation level. This is confirmed by the respective computation, which predicts a maximum value for the Rh oxidation fraction of 80%.

If we examine the experimental results gained by using the Pt/Rh/Ce catalyst, we can initially conclude that the coexistence of Rh and Ce does not have a cumulative effect as regards CO conversion after step composition changes. It is interesting to note that this behavior is also predicted by the mathematical model. In fact, Rh oxidation and oxygen storage reactions compete to consume the oxygen surplus during the short lean excursion. Due to the much higher quantity of Ce compared to Rh, Rh is more affected by this competence than is Ce. This results in a maximum Rh oxidation fraction of about 60% (compared to the 80% in the previous case).

A/F Scan

Results from selected laboratory tests are presented in this section, together with individual mathematical model runs to illustrate some aspects of catalyst behavior during composition changes.

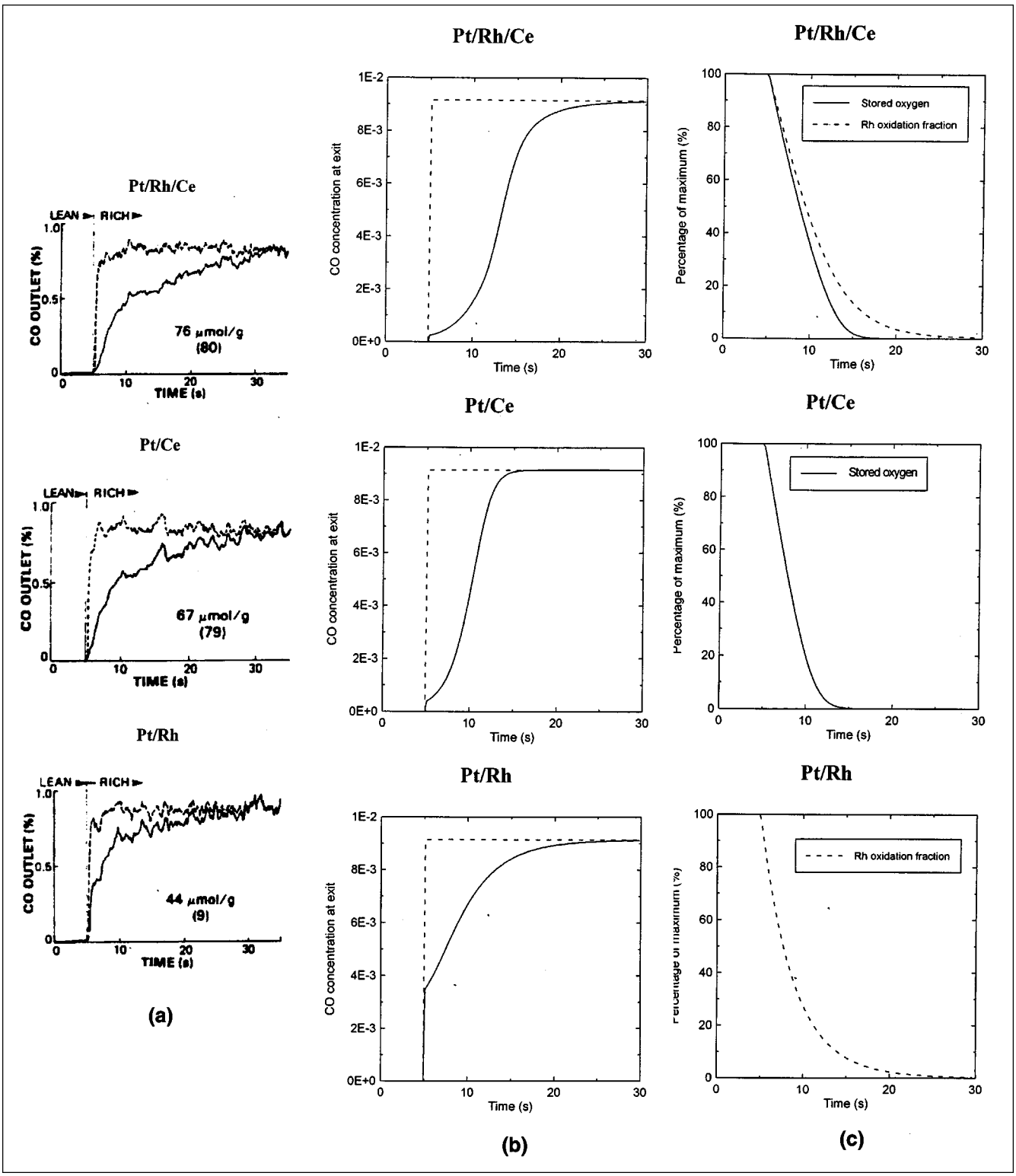

Figure 1. Step composition change response.

The A/F ratio is changed from 15.1 to 14.1. The dotted lines correspond to the expected responses if no dynamic effects were present (quasi steady state). (a) Measurements of Herz and Sell (1985); (b) and (c) computed model results.

The A/F scan test examines catalyst efficiency as a function of the A/F ratio of the feed gas at a given temperature. In this test, variations in the A/F ratio are produced by slowly changing the oxygen content of the simulated exhaust gas. In the specific test the A/F is changed from 14.5 to 15.2 in a 120-s time period. The scan is realized in both directions,

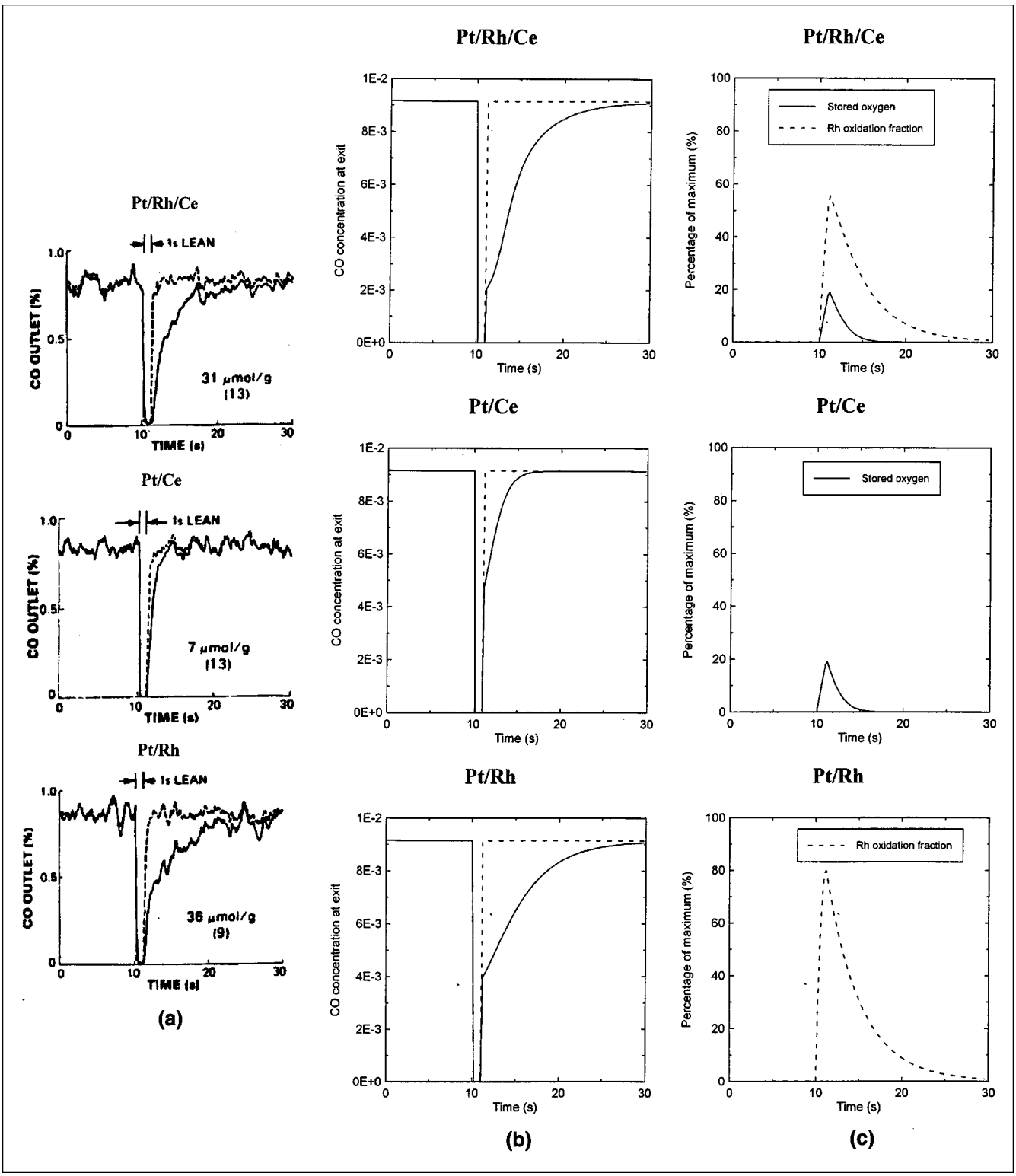

Figure 2. Lean excursion experiment.

The engine runs at a constant operation point with A/F = 14.1. A lean excursion (A/F = 15.1) is imposed for 1 s, and the engine returns to the previous rich operating point. The dotted lines correspond to the expected responses if no dynamic effects were present (quasi steady state). (a) Measurements of Herz and Sell (1985); (b) and (c) computed model results.

from rich to lean and vice versa. The feed-gas inlet temperature is kept constant at 400°C and the space velocity is 75,000 h^{-1}. Exhaust-gas composition for different A/F values in this test are given in Table 2. The geometrical and thermophysical properties of the catalytic converter are given in Appendix B.

Table 2. Exhaust Gas Composition for Selected A/F Values in the A/F Scan Experiments and Simulations

Species	Concentration (vol. %)		
	A/F = 14.5	A/F = 14.7	A/F = 15.2
CO	1	1.1	1
H_2	0.33	0.37	0.33
O_2	0.45	0.37	1.38
C_3H_6	0.05	0.05	0.05
C_3H_8	0.025	0.025	0.025
NO	0.1	0.1	0.1
H_2O	10	10	10
CO_2	14	14	14

The measured catalyst efficiency as a function of A/F for the three species of interest is presented in Figure 3. It is interesting to note that the efficiency curves are all dependent on the direction to which the A/F scan is performed. Specifically, the A/F ''window'' is wider for CO and HC when shifting from a lean to a rich environment, whereas the opposite is observed for NO. During the transition from a lean to a rich environment, the catalyst maintains a higher activity for CO and HC, which can be attributed to the previously stored oxygen. At the same time, the lower availability of CO and HC limits the NO conversion capability.

The dynamic mathematical model was employed to simulate the preceding phenomena. Figure 4 presents the computed results of the simulation of the previously described A/F scan test. It can be observed that the model can successfully describe the catalyst efficiency as a function of the A/F. Furthermore, the model predicts the dependence of catalyst efficiency on the direction of the A/F scanning. This is apparently due to the successful simulation of the dynamic phenomena (oxygen storage and water–gas reaction).

Figure 5 presents the quantity of stored oxygen and the Rh oxidation fraction during the A/F scan test, as computed by the mathematical model. After an extensive lean operation, the amount of stored oxygen is the maximum possible (60 mol/m^3 in our case). During the transition from a lean to a rich region, the stored oxygen is gradually consumed, while the storage rate is decreased. After the stored oxygen reaches a minimum value, it then starts to increase, as we move toward the lean region. The storage rate is actually higher than the release rate, which agrees with previous relative findings (Herz, 1987).

Oscillating A/F Scan

As mentioned in the Introduction, in conventional gasoline cars the catalytic converter operates at periodically oscillating A/F. The frequency and the width of the oscillation are determined by the response characteristics of the fuel-management control loop. Several often contradicting views regarding the effect of the oscillation on catalyst efficiency were expressed in the past (Cho, 1988; Muraki et al., 1985; Shinjoh et al., 1989; Cho and West, 1986). In the interesting review of Silveston (1996) it is concluded that the periodic oscillations are beneficial during the cold-start phase, when the catalyst operates at low temperatures, but they can be unfavorable at high-temperature operation. We cannot consider the preceding statement as a general rule, however, since the operating

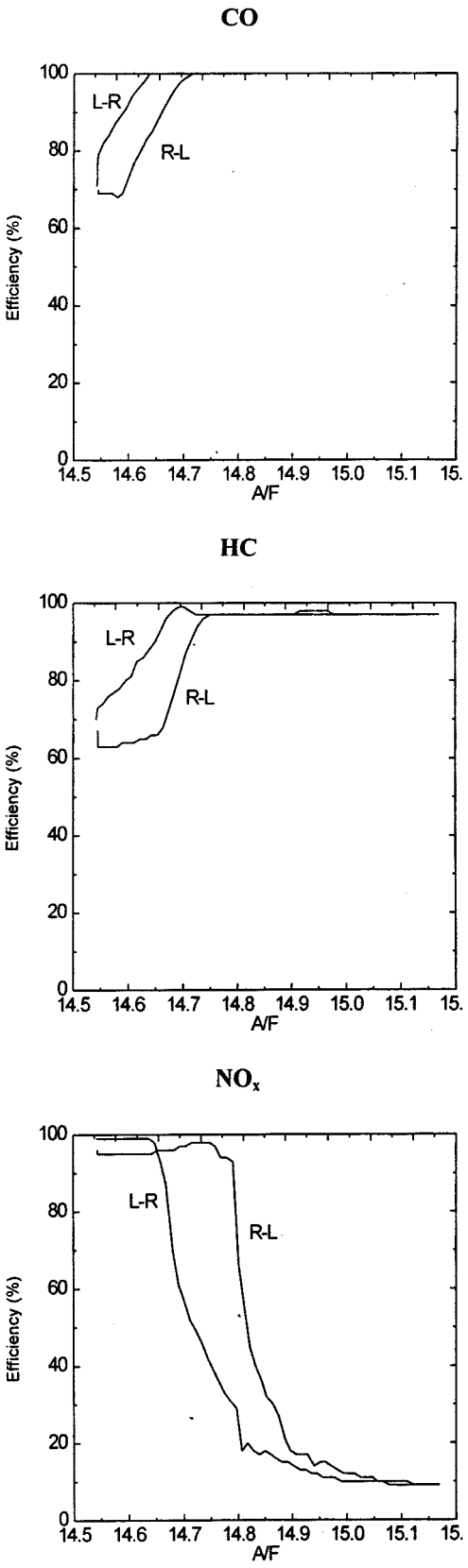

Figure 3. Measured catalyst conversion efficiency as function of A/F during transition from lean to rich environment and vice versa.

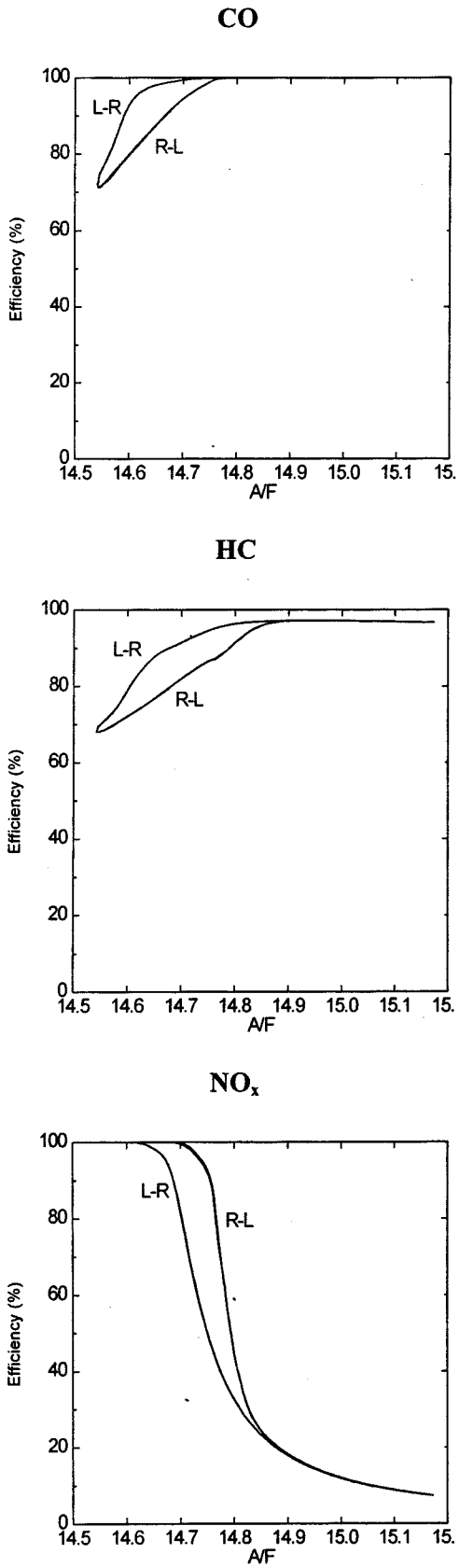

Figure 4. Computed catalyst conversion efficiency as function of A/F during transition from lean to rich environment and vice versa.

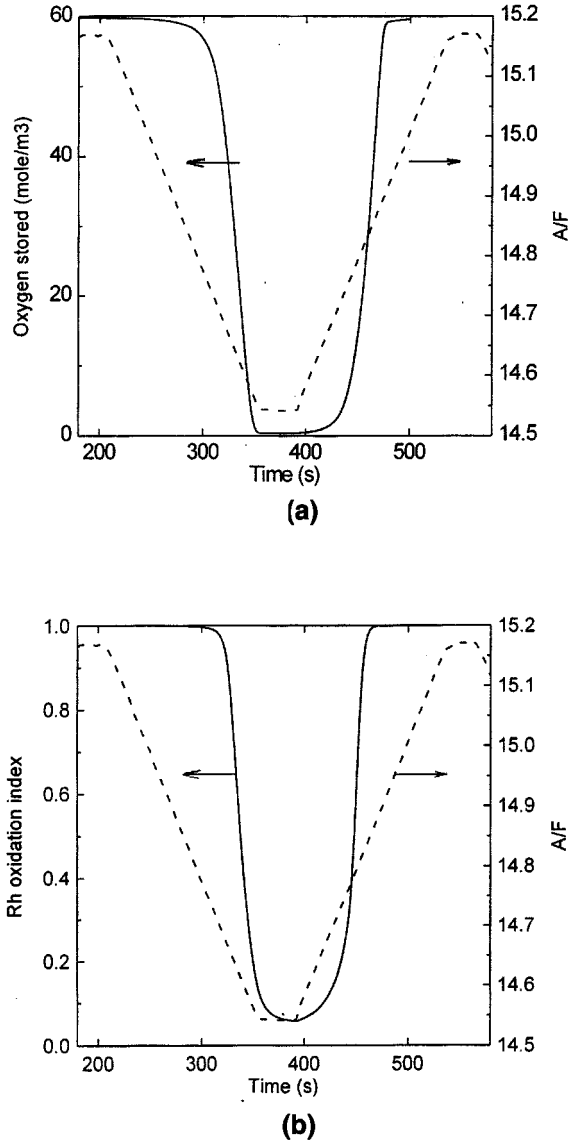

Figure 5. Computed quantity of (a) stored oxygen and (b) Rh oxidation fraction during the A/F scan test.

parameters that determine the final effect are numerous and sometimes interacting with each other. These parameters are:

- Catalyst precious-metal loading and composition;
- Loading and dispersion of oxygen storage components;
- Catalyst temperature;
- Feed-gas flow rate;
- A/F oscillation frequency;
- A/F oscillation amplitude;
- Mean value of A/F oscillation.

The number of these parameters can be even larger if we consider other possible forms of oscillation, for example, with different times in the lean and rich regions. The large number of possible combinations renders the problem of optimizing fuel management very difficult to solve. In practice, most of modern fuel-management systems try to keep A/F as close as possible to stoichiometry. Given the capabilities offered by

modern electronic control units, however, it is believed that there is a significant margin to optimize such systems by exploiting A/F oscillations.

In the following, the catalyst behavior is studied experimentally and computationally in a single A/F scan test, during which an A/F oscillation is superimposed (amplitude 0.9 A/F, frequency 0.5 Hz). The measured conversion efficiencies for the three species as functions of the mean A/F value are presented in Figure 6. We can note the following:

- As in the case with no oscillation, the efficiency depends on the direction to which the scan is realized, although the "lag" here is smaller.
- A/F oscillations result in higher CO and HC efficiencies for substoichiometric A/F; these efficiencies remain high in stoichiometry and oxygen abundance conditions. HCs especially are practically 100% converted in the whole scan range. CO efficiency at stoichiometry is 85–95%, however, compared to 100% of the no oscillation case.
- The A/F oscillation is clearly beneficial for NO conversion at lean operation and remains high in the rich region. At stoichiometry, the efficiency is significantly lower than 100%.

The results of the mathematical model in the case of the preceding experiment are given in Figure 7. In the same figure, we present the results of a simulation, without considering the dynamic submodels (oxygen storage and water–gas reaction). In fact, the latter results describe the quasi-steady behavior of the catalyst. It is obvious that the effects of the dynamic phenomena in this test are very important and actually favorable for catalyst efficiency. At the same time, we can observe that the model results compare well with the respective experimentally measured data. Of course, an exact quantitative prediction was not expected, taking into account that:

- The assumptions underlying the dynamic submodels are fairly simplistic, due to lack of sufficient kinetic studies in the field;
- To our knowledge, this is the first trial presented in the literature to predict such aspects of catalyst behavior;
- The basic aim of the work in this phase is to recognize and explain the phenomena in a qualitative way.

Figure 8 presents the stored oxygen and the Rh oxidation fraction during A/F scan with oscillation, as computed by the mathematical model. The plot refers to the computed mean values averaged over the reactor length and over a time period equal to the oscillation period. We can observe that both the stored oxygen and the Rh oxidation fraction are higher compared to the respective ones for the case with no oscillation, resulting in high oxygen availability and water–gas shift activity under rich conditions. This is explained by taking into account that the oxidation rates for the involved reactions are higher than the respective rates for the reduction reactions.

Concluding Remarks

Three-way catalytic converter operation under highly transient exhaust-gas composition changes cannot be sufficiently predicted using "quasi-steady" approaches, which are used by the majority of models presented in the literature. Mathematical models, which simulate transient adsorption–desorption phenomena, could be employed to solve the problem,

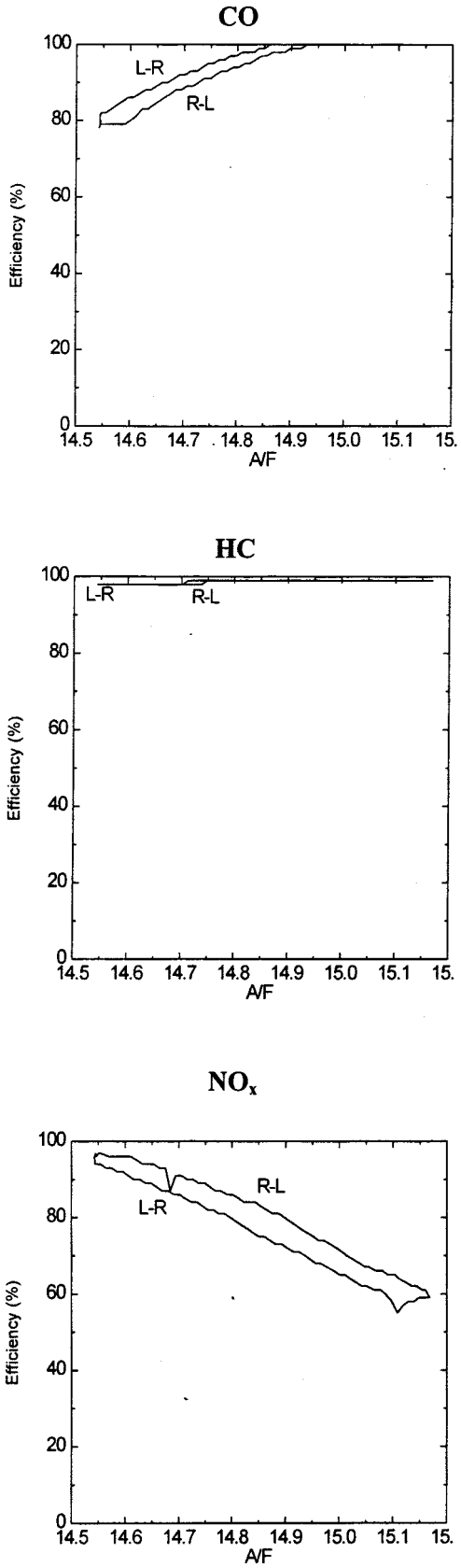

Figure 6. Measured catalyst efficiencies as functions of mean A/F value during A/F scan with superimposed oscillation.

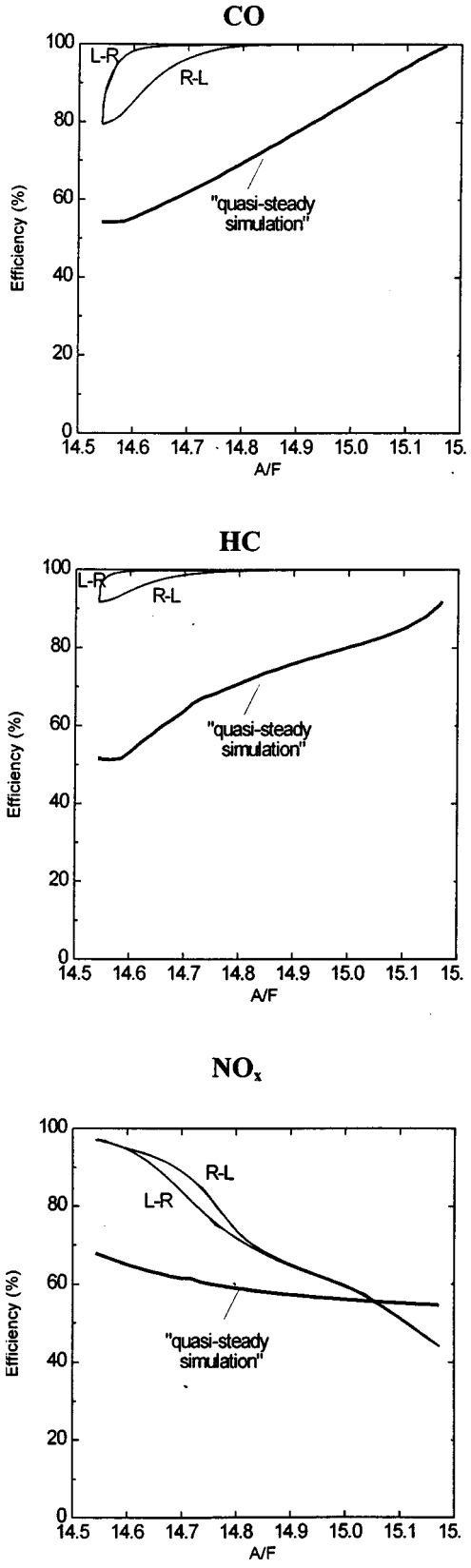

Figure 7. Computed catalyst conversion efficiencies as functions of A/F during A/F scan with oscillation; results of quasi-steady simulations are also presented.

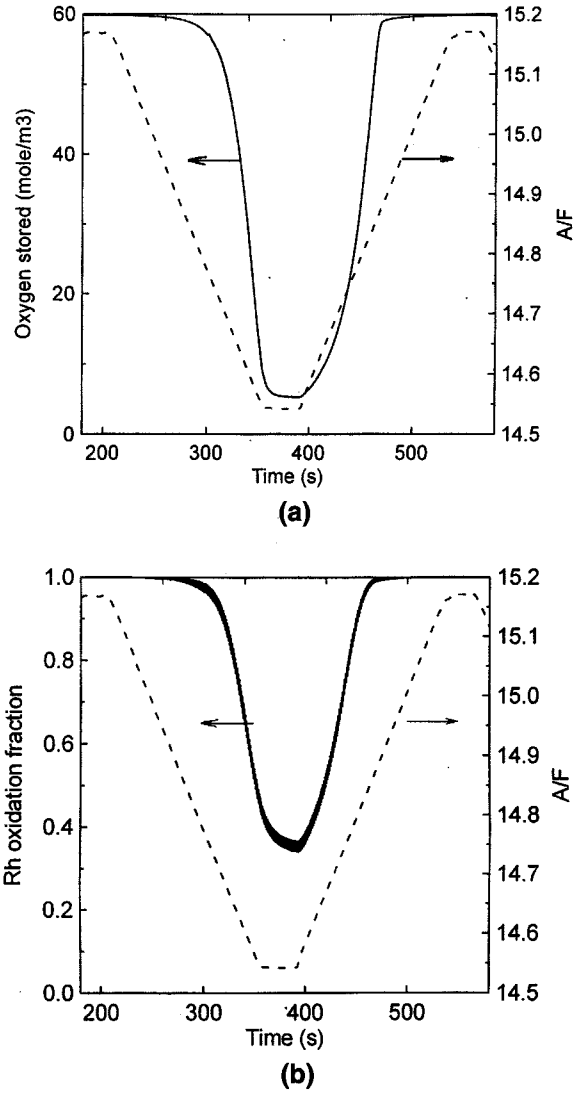

Figure 8. Computed quantity of (a) stored oxygen and (b) Rh oxidation fraction during A/F scan with oscillation.

but they are extremely demanding in terms of input data. Furthermore, the theoretical assumptions of such models are probably questionable in the automotive exhaust environment.

In this work, a quasi-steady model was equipped with dynamic submodels of the basic dynamic phenomena. Following experience cited in the literature, as well as related computational investigations, oxygen storage and transient water–gas shift activity are recognized as important dynamic phenomena and modeled with simple reaction schemes. It was concluded that the submodels offered good prediction capabilities, at least qualitatively, for a wide operating range.

A set of experimental tests and the respective model runs were used to investigate the critical aspects of 3-way catalyst transient behavior in realistic operating conditions. In the A/F scan test, a significant dependence on the scan direction was found. This was attributed to the combined action of the

dynamic phenomena and quantitatively explained by the mathematical model.

The A/F oscillation, which is of great practical interest, was investigated experimentally and computationally in a selected test case during an A/F scan. In the specific test, it was found that the oscillation was beneficial for CO and HC at rich conditions, as well as for NO at lean conditions. At stoichiometry, the conversion efficiency for all three species is slightly lower. The effects of A/F oscillations were recognized and explained with the aid of model simulations. The beneficial effect of A/F oscillations was attributed to the higher oxidation rates observed in the oxygen storage and Rh redox reactions compared to the respective reduction rates. This results in a higher level of Rh oxidation fraction as well as higher stored oxygen availability, compared to the case with no A/F oscillation.

The main objective of this work was to illustrate an alternative approach to the study and modeling of the 3WCC operation under severe transients, presenting some initial results. Further work to validate the approach in a wider field of application is scheduled. This would allow an efficient parametric analysis, whose objective would be to fine-tune the engine–converter system with optimum emission control.

Notation

A = reaction rate constant
$\bar{c}$ = vector of species concentrations, mole fraction
c = species concentration, mole fraction
C_p = specific heat capacity, J/kg·K
ΔH = heat of adsorption, J/mol
G_1 = inhibition factor due to C_3H_6 and NO, K
G_2 = inhibition factor due to CO, $K^{1.83}$
G_3 = inhibition factor due to C_2H_2
K = adsorption equilibrium constant
K_p = chemical equilibrium constant
$\dot{n}$ = molecular flux, mol/m^3·s
R = gas constant, J/mol·K
t = time, s
T = temperature, K
x = carbon atoms in the hydrocarbon molecule
y = hydrogen atoms in the hydrocarbon molecule
Ψ_{cap} = oxygen storage capacity
ψ = oxidation fraction

Subscripts

f = fast
g = exhaust gas
i = space node index
k = indication of reaction k

Literature Cited

Barbier, J., Jr., and D. Duprez, "Hydrogen Formation in Propane Oxidation on Pt-Rh/CeO_2/Al_2O_3 Catalysts," *Appl. Catal. A: Gen.*, **85**, 89 (1992).

Barshad, Y., and E. Gulari, "A Dynamic Study of CO Oxidation Over Supported Platinum," *AIChE J.*, **31**, 649 (1985).

Bozek, J. W., R. Evans, C. D. Tyree, and K. I. Zerafa, "Operating Characteristics of Zirconia Galvanic Cells (Lambda Sensors) in Automotive Closed-Loop Emission Control Systems," 920289, Soc. of Automotive Engrs., International Congress, Detroit (1992).

Cho, B. K., "Performance of Pt/Al_2O_3 Catalysts in Automobile Engine Exhaust with Oscillatory Air/Fuel Ratio," *Ind. Eng. Chem. Res.*, **27**, 30 (1988).

Cho, B. K., and L. A. West, "Cyclic Operation of Pt/Al_2O_3 Catalysts for CO Oxidation," *Ind. Eng. Chem. Fundam.*, **25**, 158 (1986).

Dictor, R., "A Kinetic Study of the Water-Gas Shift Reaction over Rh/Al_2O_3 Catalysts," *J. Catal.*, **106**, 458 (1987).

Diwell, A. F., R. R. Rajaram, H. A. Shaw, and T. J. Truex, "The Role of Ceria in Three-Way Catalysts," *Catalysis and Automotive Pollution Control II*, Elsevier, Amsterdam (1991).

Herz, R. K., and P. M. Marin, "Surface Chemistry Models of Carbon Monoxide Oxidation on Supported Platinum Catalysts," *J. Catal.*, **65**, 281 (1980).

Herz, R. K., "Dynamic Behavior of Automotive Catalysts: 1. Catalyst Oxidation and Reduction," *Ing. Eng. Chem. Prod. Res. Dev.*, **20**, 451 (1981).

Herz, R. K., J. B. Klela, and J. A. Sell, "Dynamic Behavior of Automotive Catalysts. 2. Carbon Monoxide Conversion under Transient Air/Fuel Ratio Conditions," *Ind. Eng. Chem. Prod. Res. Dev.*, **22**, 387 (1983).

Herz, R. K., and J. A. Sell, "Dynamic Behavior of Automotive Catalysts: III. Transient Enhancement of Water-Gas Shift over Rhodium," *J. Catal.*, **94**, 166 (1985).

Herz, R. K., "Dynamic Behavior of Automotive Three-Way Emission Control Systems," *Catalysis and Automotive Pollution Control*, Elsevier, Amsterdam, p. 427 (1987).

Hoebink, J. H. B. J., J. P. Huinink, and G. B. Marin, "A Quantitative Analysis of Transient Kinetic Experiments: The Oxidation of CO by O_2 over Pt," *Appl. Catal. A: Gen.*, **160**, 139 (1997).

Koltsakis, G. C., "Theoretical and Experimental Investigation of the 3-Way Catalytic Converter Dynamic Behavior," PhD Thesis, Aristotle University Thessaloniki, Thessaloniki, Greece (1996).

Koltsakis, G. C., P. A. Konstantinidis, and A. M. Stamatelos, "Development and Application Range of Mathematical Models for 3-Way Catalytic Converters," *Appl. Catal. B: Environ.*, **12**, 161 (1997).

Koltsakis, G. C., I. P. Kandylas, and A. M. Stamatelos, "Three-Way Catalytic Converter Modeling and Applications," *Chem. Eng. Commun.*, **164**, 153 (1998).

Matsunaga, S.-I., K. Yokota, H. Muraki, and Y. Fujitani, "Improvement of Engine Emissions over Three-Way Catalyst by the Periodic Operations,", Soc. of Automotive Engrs., 872098 (1987).

Muraki, H., H. Shinjoh, H. Sobukawa, K. Yokota, and Y. Fujitani, "Behavior of Automotive Noble Metal Catalysts in Cycled Feedstreams," *Ind. Eng. Chem. Prod. Res. Dev.*, **24**, 43 (1985).

Nievergeld, A. J. L., J. H. B. J. Hoebink, and G. M. Marin, "The Performance of a Monolithic Catalytic Converter of Automotive Exhaust Gas with Oscillatory Feeding of CO, NO and O_2: A Modelling Study," *Catalysis and Automotive Pollution Control III*, Elsevier, Amsterdam (1994).

Nunan, J. G., H. J. Robota, M. J. Cohn, and S. A. Bradley, "Physico-Chemical Properties of Ce-Containing Three-Way Catalysts and the Effect of Ce on Catalyst Activity," *Catalysis and Automotive Pollution Control II*, Elsevier, Amsterdam (1991).

Oh, S. H., and J. C. Cavendish, "Mathematical Modeling of Catalytic Converter Lightoff—Part III: Prediction of Vehicle Exhaust Emissions and Parametric Analysis," *AIChE J.*, **31**(6) (1985).

Oh, S. H., G. B. Fisher, J. E. Carpenter, and D. W. Goodman, "Comparative Kinetic Studies of CO-O_2 and CO-NO Reactions over Single Crystal and Supported Rhodium Catalysts," *J. Catal.*, **100**, 360 (1986).

Pattas, K. N., A. M. Stamatelos, P. K. Pistikopoulos, G. C. Koltsakis, P. A. Konstantinidis, E. Volpi, and E. Leveroni, "Transient Modeling of 3-Way Catalytic Converters," 940934, Soc. of Automotive Engrs., International Conference, Detroit (1994).

Racine, B. N., and R. K. Herz, "Modeling Dynamic CO Oxidation over Pt/Al_2O_3: Effects of Intrapellet Diffusion and Site Heterogeneity," *J. Catal.*, **137**, 158 (1992).

Schlatter, J. C., and P. J. Mitchell, "Three-Way Catalyst Response to Transients," *Ind. Eng. Chem. Prod. Res. Dev.*, **19**, 288 (1980).

Schlatter, J. C., R. M. Sinkevitch, and P. J. Mitchell, "Laboratory Reactor System for Three-Way Automotive Catalyst Evaluation," *Ind. Eng. Chem. Prod. Res. Dev.*, **22**, 51 (1983).

Shinjoh, H., H. Muraki, and Y. Fujitani, "Periodic Operation Effects in Propane and Propylene Oxidation over Noble Metal Catalysts," *Appl. Catal.*, **49**, 195 (1989).

Shulman, M. A., D. R. Hamburg, and M. J. Throop, "Comparison of Measured and Predicted Three-Way Catalyst Conversion Efficiencies under Dynamic Air-Fuel Ratio Conditions," 820276, Soc. of Automotive Engrs., International Conference, Detroit (1982).

Siemund, S., J. P. Leclerc, D. Schweich, M. Prigent, and F. Castagna, "Three-Way Monolithic Converter: Simulations versus Experiments," *Chem. Eng. Sci.*, **51**, 3709 (1996).

Silveston, P. L., ''Automotive Exhaust Catalysis: Is Periodic Operation Beneficial?'' *Chem. Eng. Sci.*, **51**, 2419 (1996).
Su, E. C., and W. G. Rothchild, ''Dynamic Behavior of Three-Way Catalysts,'' *J. Catal.*, **99**, 506 (1986).
Taylor, K. C., and R. M. Sinkevitch, ''Behavior of Automobile Exhaust Catalysts with Cycled Feedstreams,'' *Ind. Eng. Chem. Prod. Res. Dev.*, **22**, 45 (1983).

Appendix A

Reactions considered in the mathematical model:

1. $CO + 1/2\,O_2 \rightarrow CO_2$
2. $H_2 + 1/2\,O_2 \rightarrow H_2O$
3. $C_{xf}H_{yf} + (xf + yf/4)O_2 \rightarrow xfCO_2 + (yf/2)H_2O$—fast HC
4. $C_{xs}H_{ys} + (xs + ys/4)O_2 \rightarrow xsCO_2 + (ys/2)H_2O$—slow HC
5. $CO + H_2O \rightarrow CO_2 + H_2$
6. $2\,CO + 2\,NO \rightarrow 2\,CO_2 + N_2$

The rate expressions employed in the preceding reactions are the following:

$$R_1 = \frac{A_1 \cdot e^{-E_1/RT} \cdot c_{CO} \cdot c_{O_2}}{G_1(T_s, \bar{c}) \cdot G_3(T_s, c_{C_2H_2})}$$

$$R_2 = \frac{A_2 \cdot e^{-E_2/RT} \cdot c_{H_2} \cdot c_{O_2}}{G_1(T_s, \bar{c}) \cdot G_3(T_s, c_{C_2H_2})}$$

$$R_3 = \frac{A_3 \cdot e^{-E_3/RT} \cdot c_{C_{xf}H_{yf}} \cdot c_{O_2}}{G_1(T_s, \bar{c}) \cdot G_3(T_s, c_{C_2H_2})}$$

$$R_4 = \frac{A_4 \cdot e^{-E_4/RT} \cdot c_{C_{xs}H_{ys}} \cdot c_{O_2}}{G_1(T_s, \bar{c}) \cdot G_3(T_s, c_{C_2H_2})}$$

$$R_5 = \theta_{Rh} \frac{A_5 \cdot e^{-E_5/RT} \cdot c_{CO} \cdot c_{H_2O}}{G_1(T_s, \bar{c}) \cdot G_3(T_s, c_{C_2H_2})} \; Eq_5$$

$$R_6 = \frac{A_6 \cdot e^{-E_6/RT} \cdot c_{CO}^{-0.2} \cdot c_{NO}^{0.5}}{G_2(T_s, \bar{c}) \cdot G_3(T_s, c_{C_2H_2})},$$

with the following expressions accounting for the inhibition terms:

$$G_1 = T_s\left(1 + K_{a1}c_{CO} + K_{a2}c_{C_3H_6}\right)^2 \times \left(1 + K_{a3}c_{CO}^2 c_{C_3H_6}^2\right)\left(1 + K_{a4}c_{NO}^{0.7}\right)$$

$$G_2 = T_s^{-0.17}\left(T_s + K_{a5}c_{CO}\right)^2$$

$$G_3 = 1 + K_{a6} \cdot c_{C_2H_2}.$$

To account for the chemical equilibrium of the water–gas shift reaction, an additional factor is considered in the respective reaction-rate expression:

$$Eq_5 = 1 - \frac{c_{CO_2} \cdot c_{H_2}}{c_{CO} \cdot c_{H_2O} \cdot K_p(T)}$$

The following expressions are used for the adsorption equilibrium constants:

$$k_{aj} = k_{a_0 j} \exp\left[-\Delta H_{aj}/RT_s\right]; \quad j = 1 \text{ to } 6.$$

Constant	Adsorption Heat (J/mol)	Adsorption Factor $k_{a_0 j}$
K_{a1}	-7990	65.5
K_{a2}	-3×10^5	2.08×10^3
K_{a3}	-9.65×10^4	3.98
K_{a4}	3.1×10^4	4.79×10^5
K_{a5}	-5.43×10^3	1.2028×10^5 [K]
K_{a6}	-7.145×10^4	20

Reaction	Activation Energy E_i [J/mol]	Activity Factor A_i
1	95,000	2×10^{13} [mol·K/m²·s]
2	95,000	2×10^{13} [mol·K/m²·s]
3	105,000	3×10^{14} [mol·K/m²·s]
4	125,000	4×10^{14} [mol·K/m²·s]
5	105,000	6×10^8 [mol·K$^{1.83}$/m²·s]
6	70,000	5×10^6 [mol·K/m²·s]

Kinetic constants of dynamic submodels:

Preexponential Factors [mol/m²·s]	Activation Energies [J/mol]
$A_{xo} = 3\times10^5$	$E_{ox} = 90{,}000$
$A_{red,CO} = 1.5\times10^5$	$E_{red,CO} = 90{,}000$
$A_{red,HC} = 2.6\times10^5$	$E_{red,HC} = 90{,}000$
$A_{Rh,ox} = 3.5\times10^4$	$E_{Rh,ox} = 80{,}000$
$A_{Rh,red} = 2\times10^4$	$E_{Rh,red} = 80{,}000$

Appendix B

Geometric and thermophysical properties of the 3WCC employed in the experiments and computations:

Noble metal composition	Pt/Pd/Rh
Noble-metal loading	110 g/ft^3
Monolith frontal area	5.067×10^{-4} m^2
Monolith length	0.076 m
Channel density	400 channels/in^2
Substrate thickness	0.154×10^{-3} m
Washcoat-layer thickness	0.025×10^{-3} m
Substrate density	1,800 kg/m^3
Washcoat density	1,000 kg/m^3
Monolith conductivity	1.5 W/m·K
Monolith specific thermal capacity	1,020 J/kg·K
Oxygen storage capacity	60 mol/m^3

Manuscript received Sept. 22, 1998, and revision received Dec. 29, 1998.